THE JOURNAL OF COMPARATIVE NEUROLOGY 506:535–547 (2008)

Distribution of Bursting Neurons in the CA1 Region and the Subiculum of the Rat Hippocampus

TIM JARSKY, RINA MADY, BENJAMIN KENNEDY, AND NELSON SPRUSTON*
Department of Neurobiology and Physiology, Northwestern University, Evanston, Illinois 60208

ABSTRACT

We performed patch-clamp recordings from morphologically identified and anatomically mapped pyramidal neurons of the ventral hippocampus to test the hypothesis that bursting neurons are distributed on a gradient from the CA2/CA1 border (proximal) through the subiculum (distal), with more bursting observed at distal locations. We find that the well-defined morphological boundaries between the hippocampal subregions CA1 and subiculum do not correspond to abrupt changes in electrophysiological properties. Rather, we observed that the percentage of bursting neurons is linearly correlated with position in the proximal-distal axis across the CA1 and the subiculum, the percentages of bursting neurons being 10% near the CA1–CA2 border, 24% at the CA1–subiculum border, and higher than 50% in the distal subiculum. The distribution of bursting neurons was paralleled by a gradient in afterdepolarization (ADP) amplitude. We also tested the hypothesis that there was an association between bursting and two previously described morphologically distinct groups of pyramidal neurons (twin and single apical dendrites) in the CA1 region. We found no difference in output mode between single and twin apical dendrite morphologies, which was consistent with the observation that the two morphologies were equally distributed across the transverse axis of the CA1 region. Taken together with the known organization of connections from CA3 to CA1 and CA1 to subiculum, our results indicate that bursting neurons are most likely to be connected to regular spiking neurons and vice versa. J. Comp. Neurol. 506: 535–547, 2008.

Indexing terms: afterdepolarization; Ih; morphology; information channels

A series of unidirectional excitatory synaptic connections in the hippocampus forms the trisynaptic loop, which is made up of three major cell groups: granule cells, CA3 pyramidal neurons, and CA1 pyramidal cells. The trisynaptic circuit represents only one component of the information flow system in the hippocampus. It has also been established that hippocampal fields, such as the CA1, the subiculum, and the entorhinal cortex, can be further subdivided based on their patterns of connectivity (Amaral and Witter, 1995; Gigg, 2006). For example, proximal CA1 projects to the distal subiculum, whereas distal CA1 projects to proximal subiculum (Amaral and Witter, 1995). The subdivisions of hippocampal fields, based on their patterns of connectivity, have given rise to the hypothesis that different channels of information flow are segregated in the hippocampus and may ultimately be directed to different brain regions (Amaral and Witter, 1995). Information processing by distinct channels within the hippocampal circuitry raises the possibility that information might be differentially processed if neurons within these channels have different electrical properties. Thus, detailed information regarding the electrical properties of neurons within the individual channels is likely to offer insight into hippocampal information processing for particular target brain regions.

Hippocampal neurons can fire intrinsically generated bursts of action potentials, but differences in the fraction of bursting neurons have been identified between different

Grant sponsor: National Institutes of Health; Grant number: 5F31NS45437-3 (to T.J.); Grant number: NS-35180 (to N.S.); Grant number: RR-015497 (to N.S.).

*Correspondence to: Nelson Spruston, Department of Neurobiology and Physiology, Northwestern University, 2205 Tech Drive, Evanston, IL 60208-3520. E-mail: spruston@northwestern.edu

Received 7 March 2007; Revised 8 July 2007; Accepted 5 October 2007
DOI 10.1002/cne.21564
Published online in Wiley InterScience (www.interscience.wiley.com).

hippocampal regions. Reports from our laboratory and others have demonstrated that up to 16% of CA1 neurons and 68% of subicular cells are capable of firing intrinsically generated bursts of action potentials (Jensen et al., 1996; Metz et al., 2005; Staff et al., 2000; Yue et al., 2005). The abundance of bursting neurons in the hippocampus suggests that these may be critical to hippocampal information processing. Evidence from hippocampal and other cell types demonstrates that bursting may be important for neuronal signaling and plasticity (for review see Cooper, 2002; Krahe and Gabbiani, 2004; O'Mara et al., 2001). For example, presynaptic action potential bursts in rat neocortical neurons can be transmitted across synapses more reliably than isolated spikes (Lisman, 1997; Williams and Stuart, 1999). It has also been shown that postsynaptic bursting in CA1 pyramidal neurons, when paired with a single presynaptic action potential, is sufficient to induce synaptic potentiation, whereas single postsynaptic spikes failed to induce potentiation (Pike et al., 1999; see also Wittenberg and Wang, 2006). Given the importance of bursting in neuronal signaling and plasticity, the distribution of bursting neurons within hippocampal channels is likely to have an influence on information processing.

It is possible to infer the distribution of bursting neurons within separate hippocampal channels from their distribution within hippocampal subregions. However, the distribution of bursting neurons within rat hippocampal cell groups has received only modest attention. A study that characterized the intrinsic properties of rat subicular pyramidal neurons (Staff et al., 2000) found that distal neurons (nearer the presubiculum) were more likely to exhibit strong bursting than proximal neurons (closer to CA1). However, it has also been reported that neurons in the deep layers (closer to the white matter of the alveus and farther from the hippocampal fissure) are more likely to burst than superficial neurons (Greene and Mason, 1996; Greene and Totterdell, 1997), giving rise to the suggestion that there may be a gradient in bursting along the superficial-deep axis. Although it is known that CA1 neurons burst, their distribution within the rat CA1 remains undescribed. Hence, we characterized the distribution of bursting neurons in the CA1 and subiculum to distinguish between the orthogonal bursting gradients described in previous work and to determine whether the bursting gradient in the subiculum actually extends to the CA1 region.

In addition to intrinsic properties, cell morphology can play a significant role in shaping neuronal firing properties (Mainen and Sejnowski, 1996; Schaefer et al., 2003). In CA1 pyramidal neurons, two distinct morphologies, single and twin apical dendrites, have previously been described (Bannister and Larkman, 1995). Hence, we also tested whether these distinct morphologies were associated with different output modes and/or position in the CA1.

MATERIALS AND METHODS

Tissue preparation

All animal procedures were approved by the Northwestern University Animal Care and Use Committee. Male Wistar rats 15–17 days old (average age = 16 ± 0.1 days; Harlan) were used in the preparation of 300-μm transverse hippocampal slices (Leica VT 1000S slicer, Leica Microsystems) under deep halothane anesthesia according to standard procedures (Golding et al., 1999). Slices were transferred to a suspended mesh within a chamber of fresh artificial cerebrospinal fluid (ACSF), incubated at 35°C for 20–35 min, and held at room temperature until recordings were made. For recording, individual slices were held in a small chamber perfused with fresh ACSF at 1–3 ml/minute, maintained at 34°C, and visualized with an upright, fixed-stage microscope (Axioskop FS2 plus; Zeiss) using differential interference contrast infrared videomicroscopy at ×60–160 magnification.

Pyramidal neuron selection

Prior to electrophysiological recordings, pyramidal neuron somata were identified by their location in or near the cell body layer and by their pyramidal shape. Pyramidal cell identity was verified post hoc by visualization of the cell morphology using biocytin labeling. Pyramidal neurons were selected based on their large apical dendrite, the branching of the apical dendrite extending into stratum lacunosum moleculare, their triangular soma, and their multiple basal dendrites.

Dorsal-ventral recording location

Gradients that may exist in electrophysiological properties along the dorsal-ventral axis of the hippocampus could increase the variability in firing behavior observed at any position in the transverse axis if measurements were taken from slices at different dorsal-ventral positions. Therefore, only slices from a single location were selected to increase the likelihood that gradients present in the transverse axis would be observed. The position of slices along the dorsal-ventral axis in the hippocampus was obtained by measuring from the intact ventral surface of the dorsally mounted brain. Dorsal mounting was made possible via a blocking cut, which removed a section of the dorsal cortex, creating a flat surface on which to mount the brain. The blocking cut was made at a 20–30° angle between the horizontal and the sagittal planes and a 20–30° angle between the horizontal and the coronal planes. The hippocampus first appears approximately 1 mm from the ventral surface of the cortex and continues for approximately 6 mm. The average slice position along the dorsal-ventral axis used in experiments was 2.5 ± 0.1 mm from the ventral surface of the brain. Recordings were made at a pentration depth of 10–30 μm.

Anteroposterior recording locations

Multiple recordings (three to ten) were made from single slices to increase the probability that electrophysiological correlates of position would be observed. Young rat tissue was used to increase the likelihood of obtaining multiple recordings from a single slice. To facilitate subsequent anatomical mapping, recordings were made sequentially, starting proximally (near the CA2/CA1 border) and proceeding distally (toward the subiculum/entorhinal cortex border) at well separated locations. However, the position of the first recording varied across the entire proximal-distal axis of the CA1. At the time of recording, the position of each neuron was documented in an anatomical sketch and a widefield photograph. The sketch and the photograph were later used to associate the electrophysiological recording with the biocytin-labeled neuron.

Patch-clamp recordings

Current-clamp recordings were performed using bridge balance and capacitance compensation with BVC-700 amplifiers (Dagan, Minneapolis, MN). Data were filtered at 5 kHz and sampled at 100 kHz. Patch electrodes (3–6 MΩ) were made from thick-walled borosilicate glass (EN-1; Garner Glass, Claremont, CA) and filled with K-gluconate internal solution (see below). Only cells with membrane potentials negative to –55 mV on break-in were used for experiments. Membrane potential was maintained at near –70 mV with DC injection as needed. All recordings were performed at 34°C ± 1°C and were obtained in the presence of blockers of excitatory, inhibitory, and cholinergic synaptic input, i.e., 2.5 mM kynurenic acid, 2 μM SR95531 [2-(3-carboxypropyl)-3-amino-6-(4-methoxyphenyl)-pyridazinium bromide], and 1 μM atropine, respectively. After the recordings, slices were transferred to storage vials that contained fixative solution (3% paraformaldehyde in 2.5 mM phosphate buffer, pH 7.3).

Solutions and drugs

Chemicals were obtained from Sigma (St. Louis, MO). ACSF contained the following (in mM): 125 NaCl, 25 $NaHCO_3$, 2.5 KCl, 1.25 NaH_2PO_4, 25 glucose, 2 $CaCl_2$, and 1 $MgCl_2$. K-gluconate internal solution, pH 7.3, contained the following (in mM): 115 K-gluconate, 20 KCl, 10 Na-phosphocreatine, 10 HEPES, 2 Mg-ATP, 0.3 Na-GTP, and 0.1% w/v biocytin for later histological processing.

Data acquisition and analysis

Data were transferred to a computer during the experiments by an ITC-18 digital-to-analog converter (InstruTech, Port Washington, NY). Igor Pro (WaveMetrics, Lake Oswego, OR) software was used for acquisition and analysis. Statistical tests were performed in Excel (Microsoft, Redmond, WA) or GB-STAT (Dynamic Microsystems, Silver Spring, MD). All results are reported as mean ± SE, and significance was determined by Pearson correlation analysis and/or ANOVA, followed by a pairwise comparison test (Bonferroni procedure).

Measurement of electrophysiological properties

Input resistance was determined from the slope of the linear portion of the steady-state voltage vs. current plot that resulted from giving 600-msec current injections ranging from –200 to 200 pA. Threshold was defined as the point at which the change in voltage over time met or exceeded 28 mV/msec on the rising phase of the action potential, which was confirmed by eye to correspond to the inflection point at which an action potential began. Spike amplitude is reported as the difference between the peak spike voltage and the threshold. The fast afterhyperpolarization (fAHP) is reported as the membrane potential at which the change in voltage on the descending phase of the action potential met or was more than −45 mV/msec and was expressed relative to resting membrane potential. The afterdepolarization (ADP) is reported as the average membrane potential, relative to the resting membrane potential (for 50 msec before the spike), in the first 10 msec after the fAHP. Firing frequency was determined by dividing the number of action potentials induced by the duration of the current injection. The current-frequency relationship was determined by fitting a single exponential [$F = F_{max}(1 - \exp(-(I - I_0)/\iota))$] to the firing frequency response of current injections, ranging from 50 to 500 pA in 50-pA steps. F_{max} is the maximum firing frequency, I is the current, I_0 is the minimal current required to elicit spiking, and ι is the "current constant" that characterizes the exponential relation. The distinction between bursting and regular spiking responses was captured by comparing the shortest interspike interval (ISI) with the mean ISI of the response in each cell (ISI ratio = shortest ISI/average ISI) in response to 10% suprarheobase current injection (minimum 500 msec current injection required to elicit an action potential).

Anatomical mapping of recording location

Neurons filled with biocytin were processed for visualization by using an avidin-horseradish peroxidase (HRP) 3,3′-diaminobenzidine reaction. The position of each neuron was then mapped using the Neurolucida system (MicroBrightField, Williston, VT), allowing comparisons of anatomical position with electrophysiological properties (Fig. 1). Neurons were mapped in two axes: proximal-distal (following the curve of the CA cell body layer; neurons closest to the dentate gyrus (DG) are proximal) and superficial-deep (in CA1 superficially located neurons are located at the border of stratum radiatum and stratum pyramidale; deep neurons are located in the stratum oriens). To control for variations in rat brain size, a normalized scale was used in which cell position is expressed as a percentage of CA1 length. The CA2–CA1 border is at –100%, the CA1–subiculum border is at 0%, and cell positions in the subiculum are expressed as positive percentages. Borders of hippocampal subregions were determined by visual examination (Fig. 1) of the tissue after biocytin labeling. The CA2–CA1 border was marked by a relatively sharp transition from wide (in the superficial-deep axis) cell body layer to a narrower, denser band (see Fig. 2C; Amaral and Witter, 1995). The border with the subiculum was defined as the point at which the superficial cells of the pyramidal cell layer ceased to be contiguous (West et al., 1991). These visual markers were found to be consistent with current anatomical maps (Paxinos and Watson, 1998).

Data binning

Data were binned along the proximal-distal and superficial deep axis. Bin size in the proximal-distal and superficial-deep axis was 25% and 25 μM, respectively. The minimal number of points required to generate a bin was six. The average number of cells in a bin was 16 ± 2.

Control analysis

To ensure that Pearson correlation coefficient measures in one axis were not artifacts of significant relationships in the orthogonal axis, we performed several control analysis steps. When a significant relationship was observed in the proximal-distal axis, the possibility exists, because of the increase in depth of the cell body layer at more distal positions, that it is an artifact of sampling deeper cells at distal positions. Deep cells would contaminate the analysis only if they were different from superficial cells for the parameter of interest. Therefore, if there was no relationship between position in the superficial-deep axis for the same parameter, we concluded that deep cells at distal positions were not biasing the relationship observed in the proximal-distal axis. If, however, there was an association

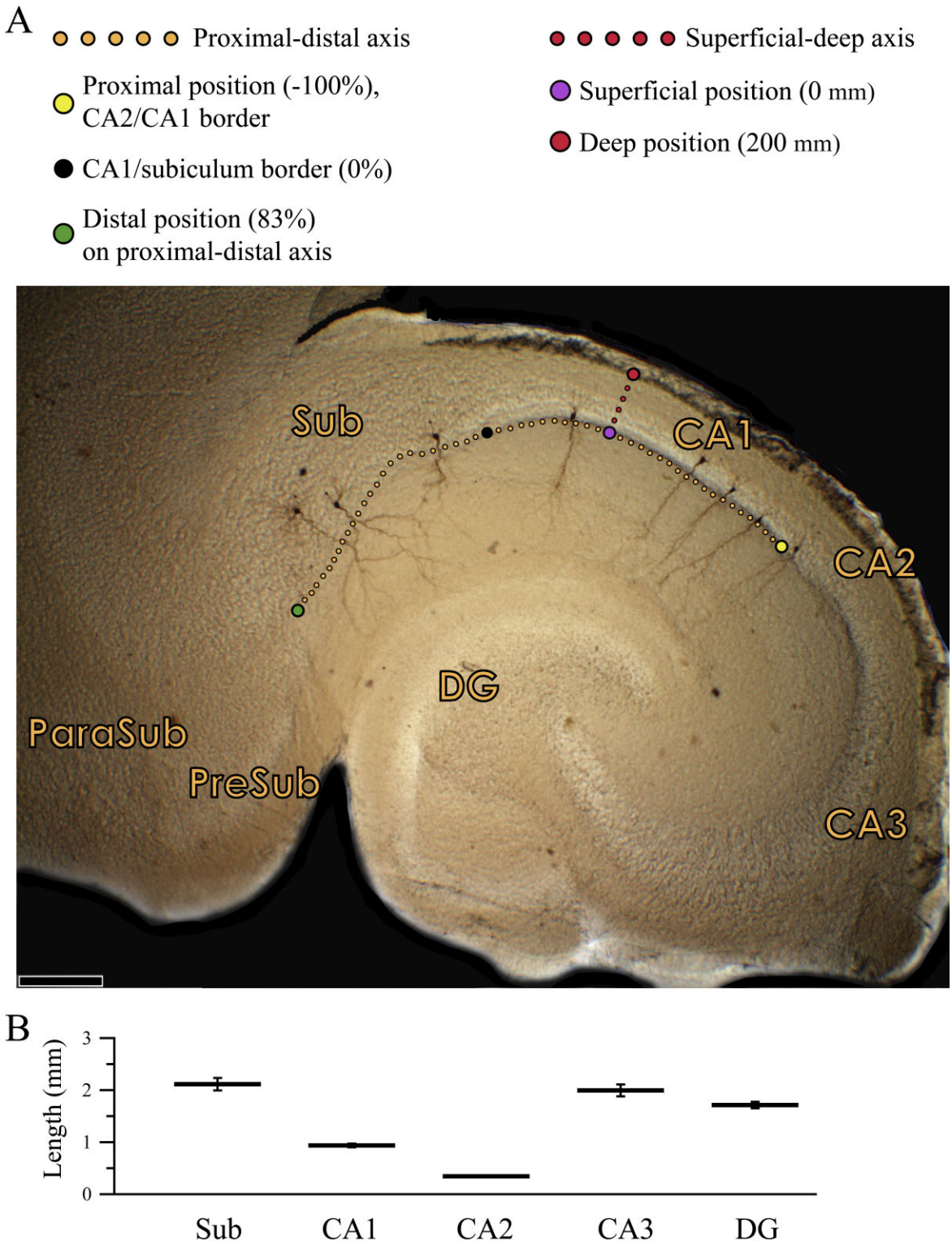

Fig. 1. Anatomical measurements of ventral hippocampus in the horizontal plane. **A:** Representative 300-μm-thick horizontal section obtained from the ventral hippocampus. Section contains eight biocytin-labeled neurons that span CA2, CA1, and the subiculum. Small orange dots mark the proximal-distal axis along the stratum radiatum–stratum pyramidale border. Large yellow dot indicates the most proximal position in CA1, at the CA2–CA1 border. Large black dot marks the CA1–subiculum border. Large green dot indicates a representative distal position in subiculum. Small red dots demarcate a representative superficial deep axis, with the large purple and red dots demarcating 0 and 200 μm on the superficial-deep axis, respectively. **B:** Average (n = 32) proximal-distal length of hippocampal formation subregions ± SEM. Scale bar = 250 μm.

in the superficial-deep axis as well as the proximal-distal, we subjected the proximal-distal correlation to a second control analysis step. Instead of sampling all the neurons along the superficial-deep axis, we sampled only superficial neurons (neurons within 25 μm of the cell body layer). Neurons within this distance of the cell body layer did not exhibit a statistically significant relationship in the superficial-deep axis; thus, if the relationship in the proximal-distal axis was maintained in superficial neurons, we considered it to be significant. Alternatively, if a significant association was observed in the superficial-deep axis, the possibility existed that it could result from CA1 neurons, which are mostly superficial, being different from subiculum neurons, which can be deeper. Therefore, we ungrouped the data and performed a correlation analysis in CA1 and subiculum cells separately. If the relationship in the superficial-deep axis persisted in the ungrouped analysis, we considered the superficial-deep axis association to be significant.

Photomicrograph production

Images were acquired on a Leica DMLB microscope (Leica, Bannockburn, IL) using a MicroFire digital CCD camera (Optronics, Goleta, CA). Image brightness and contrast were then adjusted in Photoshop CS2 (Adobe, San Jose, CA) to highlight neuronal morphology of stained neurons.

RESULTS

Intrinsic activity patterns in CA1 and subicular pyramidal neurons

We obtained 146 whole-cell patch-clamp recordings from CA1 (n = 83) and subicular (n = 63) pyramidal neurons to assess their firing behavior. CA1 and subicular pyramidal neurons had an overlapping range of intrinsic activity patterns in response to 10% supra-rheobase current injections (Fig. 2A). In agreement with with previous observations (Jung et al., 2001; Metz et al., 2005; Staff et al., 2000), we found CA1 and subicular neurons capable of producing either regular or burst spiking patterns of action potentials. Only subicular neurons were able to produce repeated bursts of action potentials in response to a single depolarizing current injection lasting for 600 msec (Fig. 2A, bottom right). We used the bimodal distribution of ISI ratio (shortest ISI/average ISI; Fig. 2B) of all pyramidal neurons as the reason to separate them into two groups: burst firing and regular spiking. Burst-firing neurons were defined as having an ISI ratio of 0.2 or less. The resting membrane potentials at break-in were not significantly different between burst-spiking and regular-spiking neurons, indicating that firing behavior was not a function of cell health.

Anatomical distribution of action-potential-bursting pyramidal neurons in the CA1 and subiculum

To test the hypothesis that the distribution of bursting neurons is continuous, we compared output mode to position along the proximal-distal and superficial-deep axes (Fig. 3A) of the ventral hippocampus. There was a statistically significant positive correlation ($r = 0.83$, $P < 0.02$, $n = 137$) between bursting and position in the proximal-distal axis of the horizontal plane (Fig. 3B). In response to

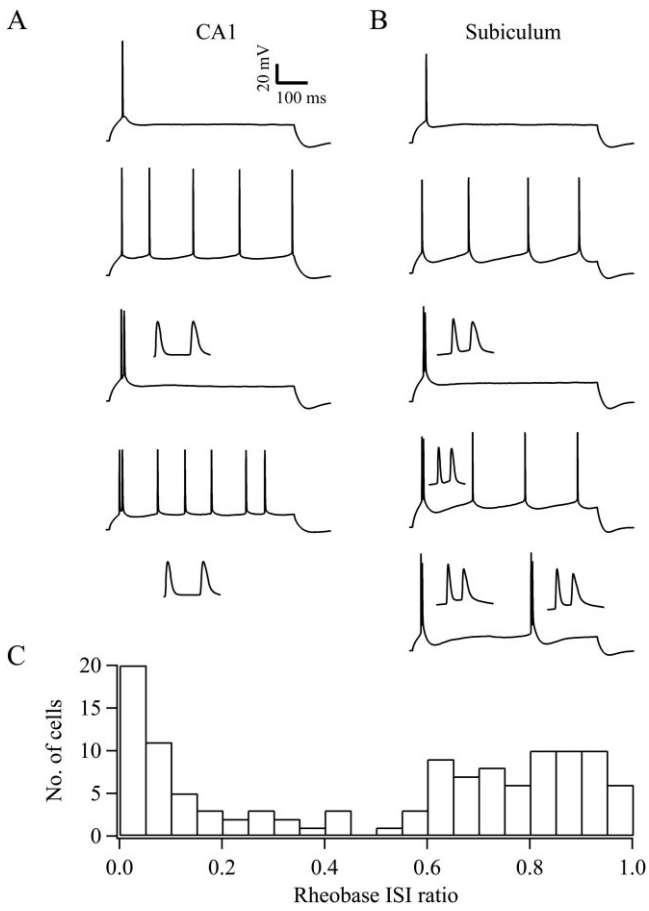

Fig. 2. Voltage responses of CA1 and subicular pyramidal neurons to 600 msec, 10% supra-rheobase current injections. **A:** CA1 voltage response. **B:** Subicular voltage response. In A and B, each trace is from a different neuron. From top to bottom: single spike, regular spiking, single burst, single burst followed by regular spiking, and multiple bursts (only in B). *Insets* show magnified view of high-frequency bursts. **C:** Histogram of ISI ratios obtained at 10% supra-rheobase for all neurons recorded from in the CA1 and subiculum. Note the bimodal distribution. Bursting neurons were defined as those having ISI ratios of 0.2 or less.

10% supra-rheobase current injections, neurons closest to the CA2–CA1 border were the least likely to burst (10%). Within CA1, the percentage of bursting neurons reached as high as 24% near the CA1–subiculum border. This linear trend continued well into distal regions of the subiculum, where more than half the neurons produced bursts. The association between bursting and position in the proximal-distal axis was maintained when only superficial neurons (within 25 μm) were considered (Fig. 3B, open circles; $r = 0.94$, $P < 0.02$, $n = 45$), demonstrating that the correlation was not an artifact of sampling deeper neurons at more distal positions. The grouped analysis (CA1 and subiculum; Fig. 3C, solid squares) along the superficial-deep axis indicated that there was also a significant correlation with bursting ($r = 0.94$, $P < 0.02$, $n = 136$). However, with ungrouped analysis (Fig. 3C, open circles = CA1, n = 79; open squares = subiculum, n = 52), the relationship broke down, signifying that the correlation found with grouped analysis was an artifact of pref-

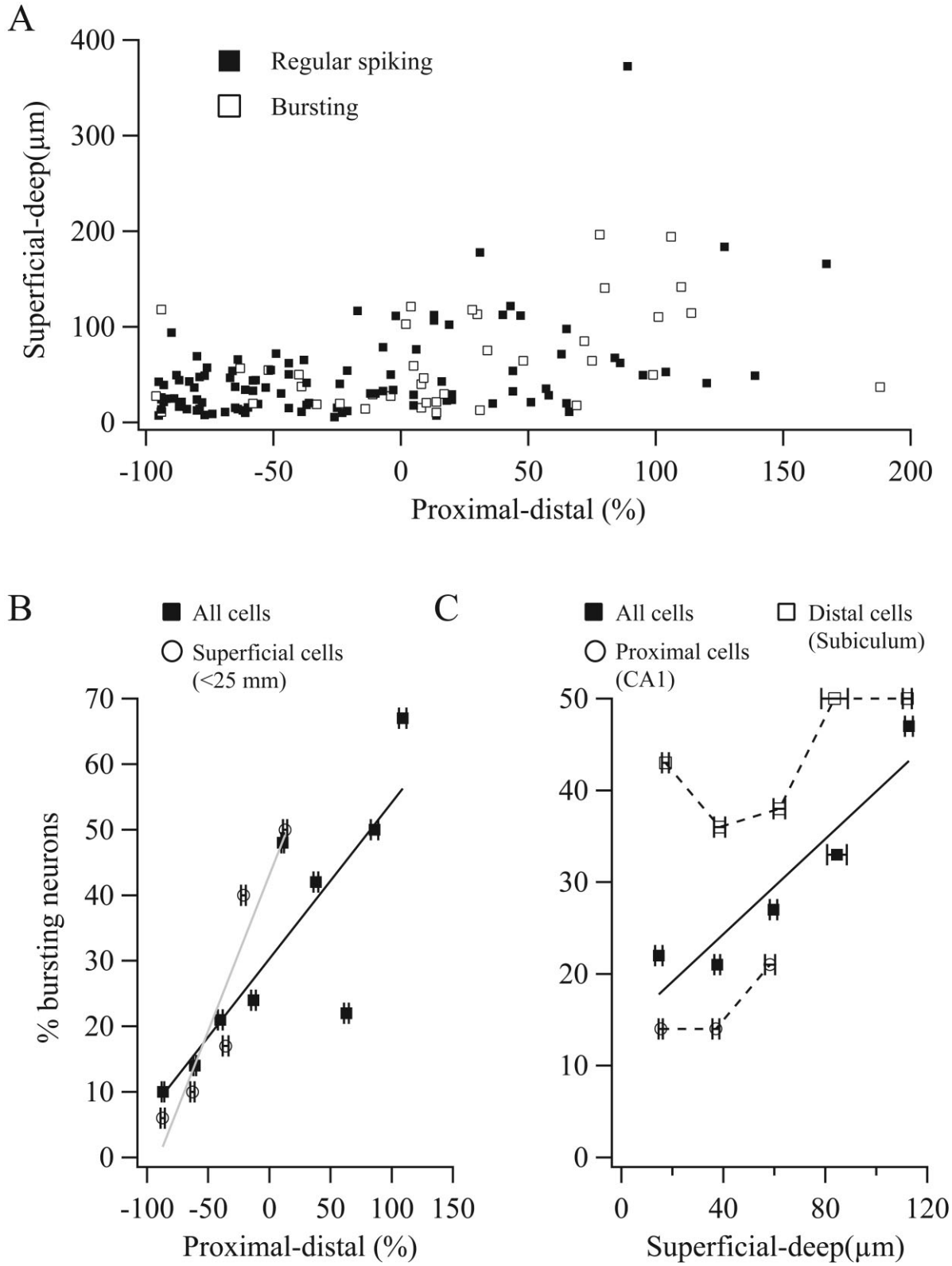

Fig. 3. Horizontal distribution of bursting pyramidal neurons in the CA1 and subiculum of the ventral hippocampus. **A:** Scatterplot of firing behavior along the proximal-distal and superficial-deep axes (n = 145). Open squares indicate bursting neurons (ISI ratio < 0.2). Solid squares indicate regular or single spiking neurons. **B:** Percentage of bursting neurons in the proximal-distal axis. Data from A were grouped into 25% bins and fit. There was a statistically significant correlation between percentage of bursting neurons and position in the proximal distal axis (solid squares; r = 0.87, $P < 0.02$, n = 137). The statistically significant correlation between percentage of bursting neurons and position in the proximal distal axis was maintained when only superficial neurons (within 25 μm) were considered (open circles; r = 0.94, $P < 0.02$, n = 45). **C:** Percentage of bursting neurons in the superficial-deep axis (solid squares). Apparent correlation (r = 0.99, $P < 0.02$, n = 136) in the superficial-deep axis was an artifact of differentially sampling distal cells at deep positions. Cell group analysis (subiculum, n = 52, open squares; CA1, n = 79, open circles) reveals no relationship between cell depth and bursting.

TABLE 1. Twelve Electrophysiological Measurements, Two Subthreshold and Ten Suprathreshold, in the Proximal-Distal and Superficial-Deep Axes

	Correlation coefficient (r)		Slope	
Property	Proximal-distal axis	Superficial-deep axis	Proximal-distal axis	Superficial-deep axis
Input resistance (MΩ/%)	–0.90**	–0.84	–0.17	—
Sag ratio (/μm)	0.53	0.97**	—	0.001
Threshold	0.42	–0.74	—	—
Max dV/dt [(mV/msec)/%]	–0.73*	–0.8	–0.19	—
Min dV/dt	–0.37	0.58	—	—
Fast AHP (mV/%)	–0.81**	0.46	–0.018	—
ADP (mV/%)	0.86**	0.039	0.018	—
Half-width (msec/%)	–0.92**	–0.46	–0.0007	—
Spike amplitude (mV/%)	–0.89**	–0.79	–0.056	—
Max firing frequency (Hz/%)	–0.84**	–0.84	–0.078	—
FI curve fit	–0.44	–0.26	—	—
Rheobase (pA/%)	0.69*	0.52	0.41	—

*$P < 0.05$.
**$P < 0.02$.

erentially sampling distal neurons at deeper positions and proximal neurons at superficial positions.

Anatomical distribution of intrinsic properties of CA1 and subicular pyramidal neurons

To test the hypothesis that differences in intrinsic properties between the CA1 and the subiculum may result from a linear gradient across the CA1 and the subiculum, we mapped 12 electrophysiological measurements, two subthreshold and ten suprathreshold, in the proximal-distal and superficial-deep axes (Table 1). We found a statistically significant correlation between anatomical position and 10 intrinsic properties. Subthreshold measures, input resistance (Fig. 4) and sag ratio (Fig. 5) varied with position but in different axes. Input resistance was lower at distal positions (46.7 ± 4.5 MΩ at 133% ± 6.0%) than near the CA2–CA1 border (95.5 ± 4.0 MΩ at –87% ± 1.2%; Fig. 4C) and did not vary in the superficial-deep axis (Fig. 4D; 87 ± 3 MΩ at 17 ± 5 μm vs. 78 ± 9 MΩ at 113 ± 2 μm). Sag ratio was larger in deep pyramidal cells (0.80 ± 0.02 at 112 ± 2 μm) than in superficial neurons (Fig. 5B; 0.71 ± 0.01 at 16 ± 0.7 μm) but did not change in the proximal-distal axis (Fig. 5A; 0.72 ± 0.01 at –87% ± 1% vs. 0.76 ± 0.02 at 109% ± 3%).

We found statistically significant suprathreshold changes along the proximal-distal axis of the horizontal plane of the ventral hippocampus in maximum dV/dt, spike amplitude, fAHP, ADP, half-width, maximum firing frequency, and rheobase (Table 1). None of these measures exhibited any relationship with position in the superficial-deep axis, so the relationship along the proximal-distal axis was considered to be real. We found a 25% change in position along the proximal-distal axis corresponded to a 6.2 mV/msec change in the maximum rate of rise, a 1.4 mV change in spike amplitude, a 0.46 mV change in fAHP amplitude, a 0.41 mV change in ADP amplitude, a 0.021 msec change in action potential half-width, a 1.6 Hz change in the maximum firing frequency, and a 10 pA change in rheobase.

Intrinsic properties of single and double apical dendrites in CA1 pyramidal neurons

To test whether an association existed between intrinsic properties and/or position in the proximal-distal axis, and the two primary apical dendrite morphologies of CA1 pyramidal neurons, we compared electrophysiological measurements from neurons that exhibited stereotyped versions (Fig. 6A) of the two morphologies. We were unable to differentiate between neurons with a single apical dendrite and those with two, for any of the measured electrophysiological parameters (Fig. 6B,C). Consistent with the observation, the two morphologies were equally distributed along the proximal-distal (mean proximal-distal position: single –56% ± 7%; double –56% ± 7%) and superficial-deep axis (mean superficial-deep position: single 37.5 ± 5 μm; double 33 ± 7 μm).

DISCUSSION

The prominence of bursting as a means of signaling in the hippocampus has raised questions regarding the distribution of bursting neurons within the hippocampal circuitry (Bilkey and Schwartzkroin, 1990; Greene and Totterdell, 1997; Masukawa et al., 1982; Staff et al., 2000). Our findings address the distribution of bursting neurons across the CA1 and the subiculum of the ventral hippocampus in young rats and demonstrate that bursting neurons are distributed along a linear gradient, with fewer bursting neurons present in the proximal CA1 region and more in the distal subiculum.

Previous reports on the distribution of bursting neurons in the subiculum are seemingly contradictory. One report shows that strong bursting pyramidal neurons, neurons that fired more than one burst during a 1-second current pulse, occur in higher percentages at distal positions in the subiculum than at proximal positions (Staff et al., 2000), whereas another study demonstrated that bursting neurons occur more frequently at deep positions than at superficial positions in the subiculum (Greene and Totterdell, 1997). Although, in agreement with Staff et al. (2000), we did not reproduce the superficial-deep differential in bursting observed by Greene and Totterdell (1997), we did not sample from neurons superficial to the pyramidal cell body layer, the region where Greene and Totterdell (1997) observed the majority of regular spiking neurons. It is the regular-spiking neurons, superficial to the cell body layer, that appear to account for the superficial-deep differences in bursting. Nevertheless, our result (no gradient in bursting from superficial to deep, obtained only from neurons located deeper than the stratum radiatum–stratum pyramidale border) shows that

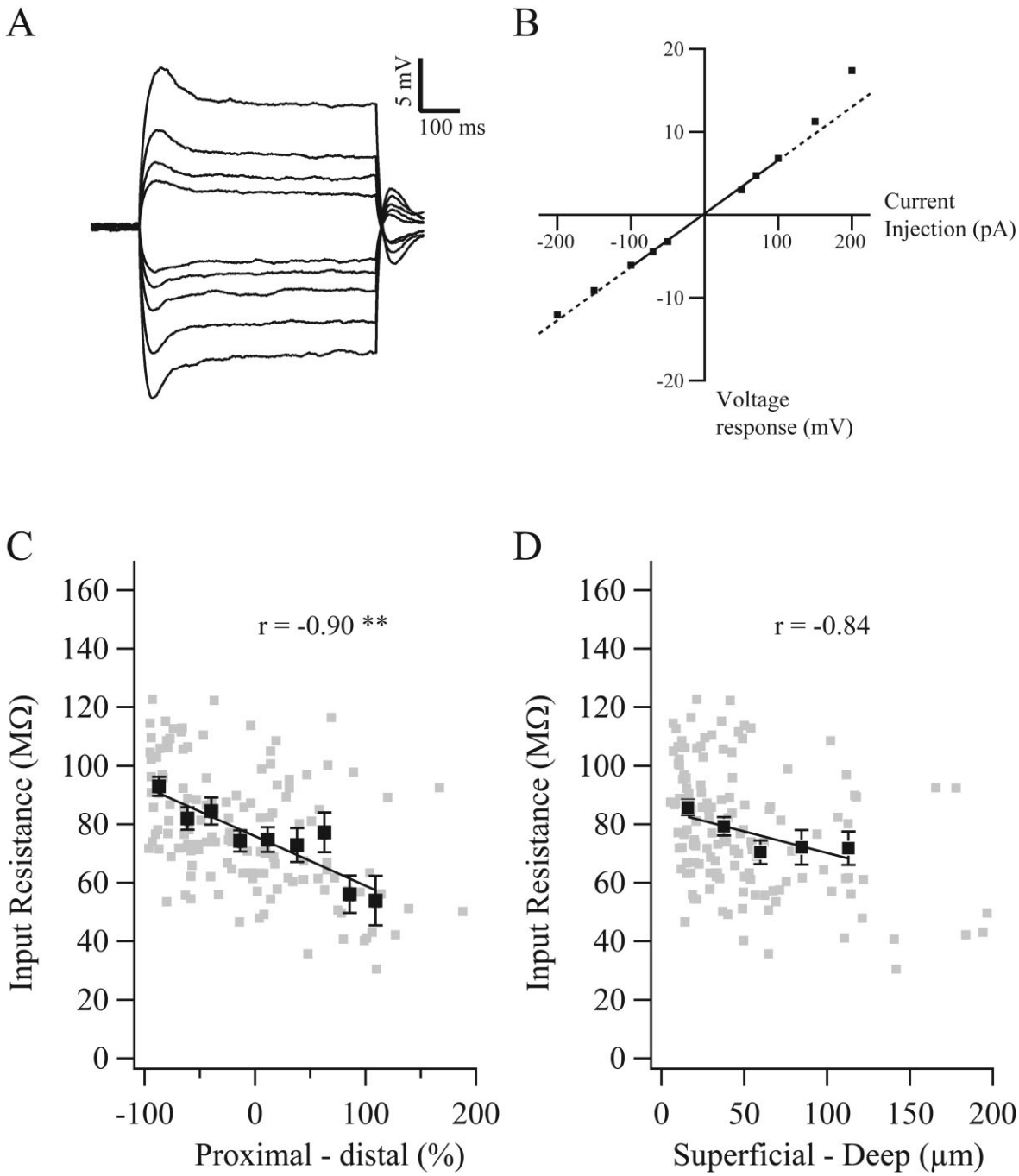

Fig. 4. Horizontal distribution of pyramidal neuron input resistance in the CA1 and subiculum of the ventral hippocampus. Distal neurons have lower input resistances than proximal neurons. **A:** Representative voltage responses to hyperpolarizing and depolarizing current steps (–200, –150, –100, –70, –50, 50, 70, 100, 150, 200 pA). **B:** Voltage-current plot. Input resistance was determined by calculating the slope of the line fit over the linear range of voltage responses. The dotted line is an extrapolation of the regression line to regions where points were not considered. **C:** Scatterplot showing relationship of input resistance to position in the proximal-distal axis ($r = -0.90$, $P < 0.02$). Gray symbols, individual neurons. Black symbols, pooled data. **D:** Scatterplot demonstrating the uncorrelated distribution of pyramidal neuron input resistance in the superficial-deep axis ($r = -0.84$, $P > 0.05$). Gray symbols, individual neurons. Black symbols, pooled data.

the differences in output mode between neurons superficial to the cell body layer and those deep to it, described by Greene and Totterdell (1997), cannot necessarily be extrapolated to infer a gradient in bursting from superficial to deep. Rather, these differences in bursting are more likely the result of sampling two different populations of neurons. Although our results are consistent with those of Staff et al. (2000), who reported that bursting neurons are

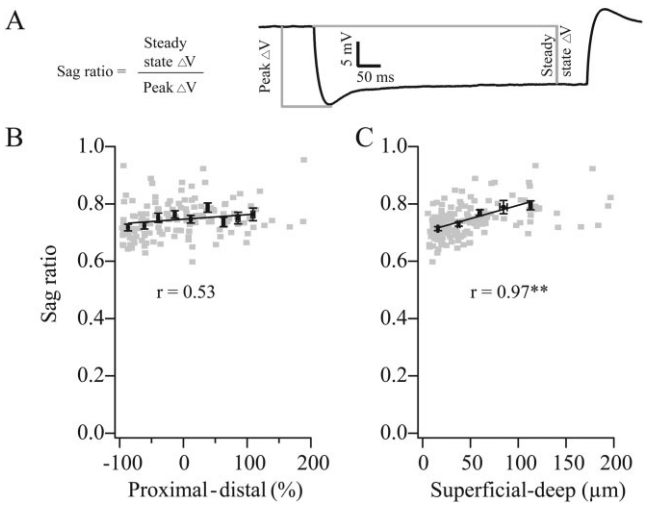

Fig. 5. Horizontal distribution of pyramidal neuron sag ratio in the CA1 and subiculum of the ventral hippocampus. Deep neurons have larger sag ratios than superficial neurons. **A:** Representative sag ratio calculation using a voltage response to a –200 pA current injection. **B:** Scatterplot emphasizing the lack of association between sag ratio and cell position in the proximal-distal axis ($r = 0.53$, $P > 0.05$). Gray symbols, individual neurons. Black symbols, pooled data. **C:** Scatterplot illustrates the significant correlation between sag ratio and cell position in the superficial-deep axis ($r = 0.97$, $P < 0.02$). Gray symbols, individual neurons. Black symbols, pooled data.

more likely to occur at distal positions, our study elucidates and expands on the results of Staff et al. (2000) in two ways. We demonstrate, first, that bursting neurons, not just strong bursting neurons, are distributed along a proximal-distal gradient in the subiculum and, second, that this gradient in the fraction of bursting neurons begins in the CA1 region.

Early work in the CA1 region of the guinea pig (Masukawa et al., 1982) using sharp electrode recordings compared the firing properties of pyramidal neurons in three regions of CA1, CA1a (distal CA1), CA1b (mid-CA1), and CA1c/CA2 (proximal CA1 and CA2; Fig. 7). Direct comparisons with our study are limited because of the combined sampling of CA1c and CA2. Nevertheless, in agreement with with our results, Masukawa et al. (1982) observed more bursting neurons in the distal CA1 (CA1a) than in the mid-CA1 (CA1b). For mid-CA1 (CA1b), they report that under 10% were found to exhibit action-potential bursting, similar to the 14% observed in our study. Although Masukawa et al. (1982) do not report the percentage of bursting neurons in CA1a, they state that bursting neurons occurred more frequently than in CA1b and that, when bursting was observed in CA1b, it tended to occur in neurons closer to CA1a. This observation is consistent with the linear increase in the percentage of bursting neurons at distal positions of CA1 observed in our study. The similarity in the distribution of bursting neurons in the rat and guinea pig hippocampus suggest that it is an evolutionarily conserved phenomenon.

In the present study, for technical reasons (see Materials and Methods), we used brain slices from young rats, which may limit the generalizability of the findings. At this early developmental stage, the percentage of bursting neurons is reduced (Chen et al., 2005). However, older animals were used in the aforementioned studies (Masukawa et al., 1982; Staff et al., 2000), which obtained results similar to ours, suggesting that the gradients we observed in electrophysiological properties may be preserved beyond the developmental stage we examined.

Distribution of intrinsic properties in the proximal-distal axis

In addition to the linear increase in the percentage of bursting neurons along the proximal-distal axis, we also observed gradients of several intrinsic properties, input resistance, maximum dV/dt, fAHP, ADP, half-width, spike amplitude, maximum firing frequency, and rheobase. The role of the ADP in driving the secondary action potentials in a burst is well established (Azouz et al., 1996; Jung et al., 2001; Metz et al., 2005; Wong and Prince, 1981; Yue et al., 2005). Therefore it is not surprising that the observed increase in the fraction of bursting neurons along the proximal-distal axis was paralleled by an increase in ADP size. The reduction in input resistance along the proximal-distal axis could also affect spiking responses, in that equivalent currents would cause smaller voltage deflections. The increase in rheobase along the proximal-distal axis is consistent with this expectation. The reduction in the maximum firing frequency, the increase in action potential half-width, and the reduction in the maximum rate of rise all appear consistent with reduced excitability. However, these measures indicate a reduction of excitability along the proximal-to-distal axis, which is not in the right direction to explain the increase in bursting observed at more distal locations. Therefore, these intrinsic differences associated with neuronal excitability, but not necessarily with bursting, appear to differentiate further the information channels within the hippocampus.

Many of the electrophysiological properties previously thought to distinguish subicular pyramidal neurons from CA1 pyramidal neurons (input resistance, spike amplitude, half-width, max. dV/dt; Staff et al., 2000) were found to be expressed along a gradient that spanned the CA1 and the subiculum. This result is somewhat surprising; we might have expected the electrophysiological properties to have changed abruptly at the CA1–subiculum border, as cell-group-specific marker genes appear to exhibit sharp transitions at cell group borders (Lein et al., 2005; Witter, 2006). The observed gradients in electrophysiological parameters give rise to the possibility that neurons close to the CA1–subicular border may be more electrically similar to adjacent neurons of the opposing cell group than neurons located farther away in the proximal-distal axis of the related cell group. The similarity of electrical properties in neurons near the border of CA1 and subiculum highlights the necessity of using both anatomical and electrical properties when assigning cell type.

Distribution of intrinsic properties in the superficial-deep axis

Analysis of intrinsic properties along the superficial-deep axis revealed a single statistically significant relationship. We found that there was less sag (larger sag ratio) in deeper neurons. Sag in the CA1 and subiculum is the result of the hyperpolarization-activated, nonselective cation current (I_h), which is active at resting membrane potentials and does not inactivate (Magee, 1998; Staff et al., 2000). It has been shown that there is an increasing density of I_h distally along the apical dendrite (Lorincz et

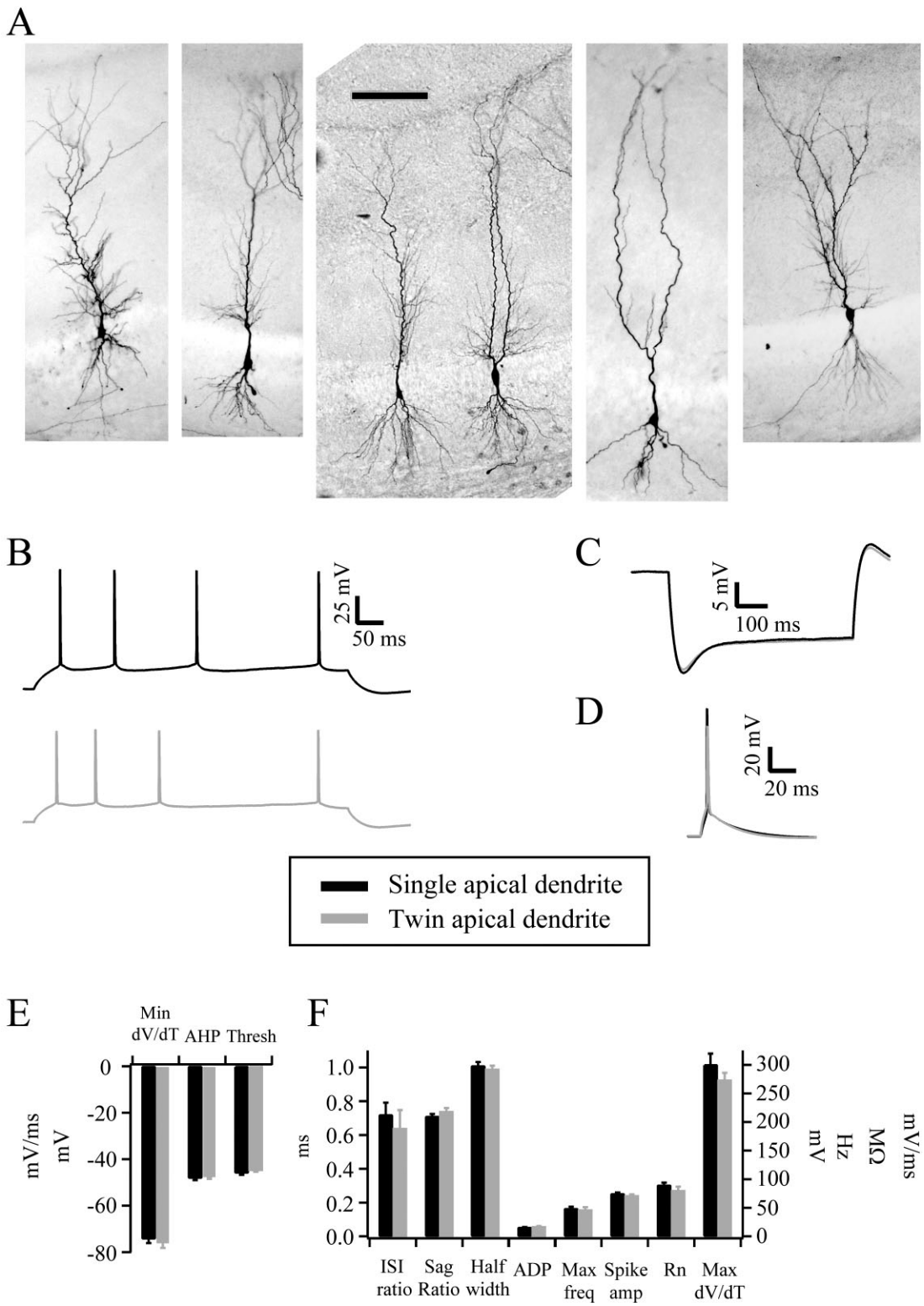

Fig. 6. Electrophysiological analysis of twin and single apical dendrite CA1 pyramidal neurons. **A:** Photographs of biocytin-labeled neurons representative of the two main apical dendrite morphologies observed in CA1. Scale bar applies to all images in A. **B–D:** Voltage responses of neurons in center panel of A. Black voltage traces from neuron with single apical dendrite. Gray voltage traces from neuron with twin apical dendrites. **B:** Voltage response to a 600 msec, 10% supra-rheobase current injection. **C:** –200 pA, 600 msec current injection. **D:** 10% Supra-rheobase, 5 msec current injection. **E,F:** Bar graphs emphasizing electrophysiological similarities between twin (n = 14) and single (n = 16) apical dendrite pyramidal neurons. No statistically significant differences were observed. Scale bar = 120 μm.

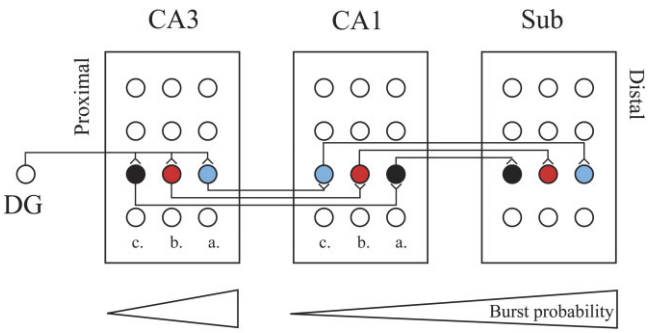

Fig. 7. Schematic diagram (modified from Amaral et al., 1991) of hippocampal cell group connectivity and bursting. Rectangles represent the CA3, CA1, and subiculum. For each field, the proximal portion is to the left of the rectangle. Each mossy fiber from a granule cell of the dentate gyrus (DG) makes several "en passant" synapses on CA3 pyramidal neurons throughout the horizontal extent of CA3. However, from this point onward, intrinsic connections are constrained by the origin cell's proximal-distal position. By following circles of the same color through the circuit, the potential for information channeling in the hippocampus is revealed. Triangles (bottom), represent a qualitative scale, with the width of the triangle at each position corresponding to the proportion of bursting neurons. a–c Denote the different subregions described by Masukawa et al. (1982).

al., 2002; Magee, 1998). Thus, one explanation for our result that neurons at similar depths had similar sag ratios is that the I_h density at one depth in the superficial-deep axis is similar for all neurons. This would indicate that the source of the I_h gradient is extracellular rather than internally generated from subcellular compartmental cues as has been previously suggested (Lorincz et al., 2002). The fact that we did not observe a difference in sag ratio between the CA1 and the subiculum is somewhat surprising, insofar as the strongest immunolabeling for the I_h channel subunit HCN1 is found in the subiculum (Lorincz et al., 2002). One possible explanation is that the portion of the resting input conductance attributable to I_h is less in the subiculum than in the CA1 (Staff et al., 2000), thereby requiring greater I_h density to achieve the same sag ratio. However, the relationship between sag ratio and I_h density is complex, and it might not be possible to predict I_h density directly from sag ratio (Staff et al., 2000). The observation that sag ratio, and hence I_h, was not associated with position in the proximal-distal axis suggests that it does not serve to differentiate hippocampal information channels. Finally, I_h has been implicated in burst generation in thalamic relay and dorsal root ganglion neurons (Deschenes et al., 1982; Jahnsen and Llinas, 1984; White et al., 1989). The orthogonal gradients of bursting and sag ratio observed here, however, suggest that I_h might not be involved in burst generation in CA1 and subicular pyramidal neurons.

Single vs. twin apical dendrites

Studies that attempt to elucidate the mechanism of firing behavior in the hippocampus have primarily assessed the contribution of ion channels (Jensen et al., 1994; Jung et al., 2001; Magee and Carruth, 1999; Metz et al., 2005; Su et al., 2001; Wong and Prince, 1978). One of the earliest studies that highlighted the contribution of neuronal morphology to action potential bursting was completed by Mainen and Sejnowski (1996). This study demonstrated that changes in morphology can transform the firing behavior of a neuron from regular spiking to bursting (Mainen and Sejnowski, 1996). In the present study, however, analysis of the intrinsic properties from somatic patch-clamp recordings of single and twin apical dendrite pyramidal neurons in CA1 failed to reveal any measurable differences. We can conclude, based on these findings, that single and twin apical dendrites do not contribute to the association between intrinsic properties and position described previously. We recognize that considering the influence of only a single morphological variable does not rule out the influence of other morphological differences.

The electrophysiological similarities between single and twin apical dendrite morphologies are consistent with the observation that they were equally distributed in horizontal section of CA1. Similar input resistance measurements of the two morphologies suggest that the impedance sum of the daughter branches of neurons with split apical dendrites is the same as the impedance of single apical dendrites. Matching impedances could indicate that the diameter of the daughter branches in twin trunks, compared with neurons with single apical dendrites, obeys the three-halves power law (Rall, 1959). Bannister and Larkman (1995) observed that the twin trunks were significantly smaller in diameter, at a given level in stratum radiatum, than single trunks, which is consistent with this possibility. However, precise measurements of dendrite diameters would be required to confirm this hypothesis.

The distribution of bursting neurons and hippocampal circuitry

The distribution of bursting neurons in the hippocampus is particularly interesting in the context of CA1–subicular connectivity (Fig. 7). Hippocampal cell group connectivity is not diffuse (Amaral et al., 1991; Gigg, 2006). In a diffuse connectivity scheme, a neuron in CA1 would have equal probability of connecting with all the neurons in the subiculum at the same dorsal-ventral location. In fact, however, subfields of hippocampal cell groups target selected subfields of connected cell groups. Specifically, the proximal CA1 projects to the distal subiculum, and the distal CA1 projects to the proximal subiculum. The implication is that the proximal CA1, where most neurons spike regularly, projects to a region where almost 60% of neurons burst. The distal CA1, where approximately one-fourth of the neurons burst, is connected to the proximal subiculum, where about one-third of the neurons burst. This association between connectivity and bursting reduces the likelihood and number of CA1–subiculum cell pairs where both neurons burst.

A similar pattern of connectivity between bursting and nonbursting neurons appears to hold for CA3-to-CA1 connections (Fig. 7). Two studies have shown that distal neurons of CA3 (CA3a) that connect with proximal CA1 neurons, burst more readily than proximal CA3 neurons that connect to distal CA1 cells (Bilkey and Schwartzkroin, 1990; Wittner and Miles, 2006). Combining these results with ours, it appears that information within the trisynaptic loop is processed differentially, depending on the population of CA3 neurons activated by the dentate gyrus. Proximal CA3 neurons burst less but project to relatively strongly bursting neurons within CA1, which in turn project to relatively weakly bursting neurons in the sub-

iculum. In contrast, distal CA3 neurons burst more but project to relatively weakly bursting CA1 neurons, which in turn project to strongly bursting neurons in subiculum (Fig. 7). Thus, within each subregion of the hippocampus, different streams of information may be influenced by bursting to different degrees. These different processing streams in turn influence different targets, as proximal, middle, and distal subiculum project to distinct extrahippocampal regions (Amaral and Witter, 1995).

The direct entorhinal cortex input to the CA1 also exhibits a transverse topographical organization (Witter, 2006). In the rat, the medial and caudal portions of the entorhinal cortex terminate primarily in proximal CA1 and distal subiculum, while more lateral and rostral portions of the entorhinal cortex project to progressively more distal portions of the CA1 and proximal subiculum (Steward, 1976; Witter and Amaral, 1991). Thus, it seems that the medial entorhinal cortex is projecting to regions of the CA1 with the lowest burst propensity and regions of subiculum with the most bursting. In contrast, lateral entorhinal cortex terminates in regions of the CA1 with the highest burst propensity and regions of subiculum with less bursting.

We have argued that our work has implications for the information processing and patterns of activity reaching different targets of the hippocampus. Such conclusions, however, are limited to a gradient along the transverse axis of the ventral hippocampus. Whether such a gradient exists in more dorsal hippocampus or whether other functional gradients exist along the dorsal-ventral (septotemporal) axis remains an open question. Future studies addressing this issue will be important, because there is good evidence for distinct anatomical projections and functions of dorsal and ventral subiculum (Gigg, 2006; O'Mara, 2005, 2006a and b). Specifically, dorsal hippocampus may be involved in relating spatial information to cortical areas, whereas ventral areas may be more closely related to hippocampal inhibition of the hypothalamic-pituitary-adrenal (HPA) axis (O'Mara, 2005, 2006a and b). Therefore, future work that maps the intrinsic changes in the dorsal-ventral axis may help to shed light on the properties of separate groups of neurons primarily affecting spatial memory and the hippocampal response to stress (Herman and Mueller, 2006).

ACKNOWLEDGMENTS

The authors thank Dr. Indira Raman and Teresa Aman for their advice and critical reading of the manuscript.

LITERATURE CITED

Amaral DG, Witter, MP. 1995. Hippocampal formation. In: Paxinos G, editor. The rat nervous system, 2nd ed. San Diego: Academic Press.

Amaral DG, Dolorfo C, Alvarez-Royo P. 1991. Organization of CA1 projections to the subiculum: a PHA-L analysis in the rat. Hippocampus 1:415–435.

Azouz R, Jensen MS, Yaari Y. 1996. Ionic basis of spike after-depolarization and burst generation in adult rat hippocampal CA1 pyramidal cells. J Physiol 492:211–223.

Bannister NJ, Larkman AU. 1995. Dendritic morphology of CA1 pyramidal neurones from the rat hippocampus: I. Branching patterns. J Comp Neurol 360:150–160.

Bilkey DK, Schwartzkroin PA. 1990. Variation in electrophysiology and morphology of hippocampal CA3 pyramidal cells. Brain Res 514:77–83.

Chen S, Yue C, Yaari Y. 2005. A transitional period of Ca^{2+}-dependent spike afterdepolarization and bursting in developing rat CA1 pyramidal cells. J Physiol 567:79–93.

Cooper DC. 2002. The significance of action potential bursting in the brain reward circuit. Neurochem Int 41:333–340.

Deschenes M, Roy JP, Steriade M. 1982. Thalamic bursting mechanism: an inward slow current revealed by membrane hyperpolarization. Brain Res 239:289–293.

Gigg J. 2006. Constraints on hippocampal processing imposed by the connectivity between CA1, subiculum and subicular targets. Behav Brain Res 174:265–271.

Golding NL, Jung HY, Mickus T, Spruston N. 1999. Dendritic calcium spike initiation and repolarization are controlled by distinct potassium channel subtypes in CA1 pyramidal neurons. J Neurosci 19:8789–8798.

Greene JR, Mason A. 1996. Effects of somatostatin and related peptides on the membrane potential and input resistance of rat ventral subicular neurons, in vitro. J Pharmacol Exp Ther 276:426–432.

Greene JR, Totterdell S. 1997. Morphology and distribution of electrophysiologically defined classes of pyramidal and nonpyramidal neurons in rat ventral subiculum in vitro. J Comp Neurol 380:395–408.

Herman JP, Mueller NK. 2006. Role of the ventral subiculum in stress integration. Behav Brain Res 174:215–224.

Jahnsen H, Llinas R. 1984. Ionic basis for the electro-responsiveness and oscillatory properties of guinea-pig thalamic neurones in vitro. J Physiol 349:227–247.

Jensen MS, Azouz R, Yaari Y. 1994. Variant firing patterns in rat hippocampal pyramidal cells modulated by extracellular potassium. J Neurophysiol 71:831–839.

Jensen MS, Azouz R, Yaari Y. 1996. Spike after-depolarization and burst generation in adult rat hippocampal CA1 pyramidal cells. J Physiol 492:199–210.

Jung HY, Staff NP, Spruston N. 2001. Action potential bursting in subicular pyramidal neurons is driven by a calcium tail current. J Neurosci 21:3312–3321.

Krahe R, Gabbiani F. 2004. Burst firing in sensory systems. Nat Rev Neurosci 5:13–23.

Lein ES, Callaway EM, Albright TD, Gage FH. 2005. Redefining the boundaries of the hippocampal CA2 subfield in the mouse using gene expression and 3-dimensional reconstruction. J Comp Neurol 485:1–10.

Lisman JE. 1997. Bursts as a unit of neural information: making unreliable synapses reliable. Trends Neurosci 20:38–43.

Lorincz A, Notomi T, Tamas G, Shigemoto R, Nusser Z. 2002. Polarized and compartment-dependent distribution of HCN1 in pyramidal cell dendrites. Nat Neurosci 5:1185–1193.

Magee JC. 1998. Dendritic hyperpolarization-activated currents modify the integrative properties of hippocampal CA1 pyramidal neurons. J Neurosci 18:7613–7624.

Magee JC, Carruth M. 1999. Dendritic voltage-gated ion channels regulate the action potential firing mode of hippocampal CA1 pyramidal neurons. J Neurophysiol 82:1895–1901.

Mainen ZF, Sejnowski TJ. 1996. Influence of dendritic structure on firing pattern in model neocortical neurons. Nature 382:363–366.

Masukawa LM, Benardo LS, Prince DA. 1982. Variations in electrophysiological properties of hippocampal neurons in different subfields. Brain Res 242:341–344.

Metz AE, Jarsky T, Martina M, Spruston N. 2005. R-type calcium channels contribute to afterdepolarization and bursting in hippocampal CA1 pyramidal neurons. J Neurosci 25:5763–5773.

O'Mara S. 2005. The subiculum: what it does, what it might do, and what neuroanatomy has yet to tell us. J Anat 207:271–282.

O'Mara S. 2006a. Controlling hippocampal output: the central role of subiculum in hippocampal information processing. Behav Brain Res 174:304–312.

O'Mara S. 2006b. Integrating the subiculum into hippocampal formation circuitry and the control of instrumental behavior: theoretical comment on Andrzejewski, Spencer, and Kelley (2006). Behav Neurosci 120:739–743.

O'Mara SM, Commins S, Anderson M, Gigg J. 2001. The subiculum: a review of form, physiology and function. Prog Neurobiol 64:129–155.

Paxinos G, Watson C. 1998. The rat brain in stereotaxic coordinates. San Diego: Academic Press.

Pike FG, Meredith RM, Olding AW, Paulsen O. 1999. Rapid report: postsynaptic bursting is essential for "Hebbian" induction of associa-

tive long-term potentiation at excitatory synapses in rat hippocampus. J Physiol 518:571–576.

Rall W. 1959. Branching dendritic trees and motoneuron membrane resistivity. Exp Neurol 1:491–527.

Schaefer AT, Larkum ME, Sakmann B, Roth A. 2003. Coincidence detection in pyramidal neurons is tuned by their dendritic branching pattern. J Neurophysiol 89:3143–3154.

Staff NP, Jung HY, Thiagarajan T, Yao M, Spruston N. 2000. Resting and active properties of pyramidal neurons in subiculum and CA1 of rat hippocampus. J Neurophysiol 84:2398–2408.

Steward O. 1976. Topographic organization of the projections from the entorhinal area to the hippocampal formation of the rat. J Comp Neurol 167:285–314.

Su H, Alroy G, Kirson ED, Yaari Y. 2001. Extracellular calcium modulates persistent sodium current-dependent burst-firing in hippocampal pyramidal neurons. J Neurosci 21:4173–4182.

West MJ, Slomianka L, Gundersen HJ. 1991. Unbiased stereological estimation of the total number of neurons in thesubdivisions of the rat hippocampus using the optical fractionator. Anat Rec 231:482–497.

White G, Lovinger DM, Weight FF. 1989. Transient low-threshold Ca^{2+} current triggers burst firing through an afterdepolarizing potential in an adult mammalian neuron. Proc Natl Acad Sci U S A 86:6802–6806.

Williams SR, Stuart GJ. 1999. Mechanisms and consequences of action potential burst firing in rat neocortical pyramidal neurons. J Physiol 521:467–482.

Wittenberg GM, Wang SS. 2006. Malleability of spike-timing-dependent plasticity at the CA3-CA1 synapse. J Neurosci 26:6610–6617.

Witter MP. 2006. Connections of the subiculum of the rat: topography in relation to columnar and laminar organization. Behav Brain Res 174: 251–264.

Witter MP, Amaral DG. 1991. Entorhinal cortex of the monkey: V. Projections to the dentate gyrus, hippocampus, and subicular complex. J Comp Neurol 307:437–459.

Wittner L, Miles R. 2006. Electrophysiological and anatomical properties underlying the pacemaker role of the hippocampal CA3a region in the generation of disinhibition-induced synchrony. Atlanta: Society for Neuroscience. p 796.

Wong RK, Prince DA. 1978. Participation of calcium spikes during intrinsic burst firing in hippocampal neurons. Brain Res 159:385–390. Wong RK, Prince DA. 1981. Afterpotential generation in hippocampal pyramidal cells. J Neurophysiol 45:86–97.

Yue C, Remy S, Su H, Beck H, Yaari Y. 2005. Proximal persistent Na^{+} channels drive spike afterdepolarizations and associated bursting in adult CA1 pyramidal cells. J Neurosci 25:9704–9720.